Received: Added at production | Revised: Added at production | Accepted: Added at production

DOI: xxx/xxxx

ORIGINAL ARTICLE

Limit-Cycle-Oscillation in DC Bus System and Its Death Through Heterogeneous Coupling

Sanjeet Kumar Subudhi*[1] | Somnath Maity[2] | Abdelali El Aroudi[3]

[1]Department of Electrical Engineering, National Institute of Technology Rourkela, Odisha, India, Email: sanjeetsubudhi@yahoo.com

[2]Department of Electrical Engineering, National Institute of Technology Rourkela, Odisha, India, Email: somnatheeiitkgp@ieee.org, somnathm@nitrkl.ac.in

[3]Departament d́Enginyeria Electrónica, Eléctrica i Virgili, Automática, Escola Técnica Superior d́Enginyeria, Universitat Rovira i Virgili, 43007 Tarragona, Spain, Email:abdelali.elaroudi@urv.cat

Correspondence
*Sanjeet Kumar Subudhi, National Institute of Technology Rourkela. Email: sanjeetsubudhi@yahoo.com

Abstract

Stability of a complex DC bus system (DBS) is a significant design consideration because of its constant power load (CPL) characteristics of the tightly-regulated load converter. In this paper, the dynamic properties of a stand-alone buck-type DBS are investigated based upon the closed-form large-signal-averaged model. The stability-analysis-in-large around the operation point shows that CPLs create a destabilizing effect on the system that can lead to severe voltage oscillation caused by discontinuity-induced Hopf bifurcations, which are qualitatively different from the bifurcations we know for smooth dynamical systems. Instead, this paper also explores the application of "amplitude death (AD) technique" to stabilize the coupled oscillatory DBSs and show that how this technique with its necessary modifications, e.g., the heterogeneity-induced AD technique characterized by two or more coupled DBSs with mismatched frequency of oscillations can provide an efficient open-loop control solution for stabilizing the coupled DBSs. Finally, simulations and experimental results are provided to validate all these concepts.

KEYWORDS:
DC power systems; limit cycle oscillation (LCO); discontinuity-induced Hopf bifurcation (DIHB); amplitude death (AD); heterogeneous coupling; stability analysis.

1 | INTRODUCTION

Recently, DC distribution power systems consisting of networks of self-controlled switching power converters have become increasingly common in various practical applications, such as in VLSI mainframe computers' power supplies[1], telecommunication systems[2], electric vehicles[3], and modern DC microgrids[4]. Advantages of DC bus systems (DBSs) are mainly power interfacing flexibility attributed to reduced size and weight, high-efficiency energy conversion, simple implementation of power source paralleling, easy incorporation of DC-type renewable resources, and ability to satisfy a variety of control objectives[5]. However, major problem for such a DC distribution is its potential stability degradation that can occur when switching converters are connected to a common DC bus voltage. This destabilizing effect can happen because of the negative impedance property of the load-side converter[6] and hence leading to undesirable low-frequency oscillation — called also limit cycle oscillation (LCO)[7,8,9]. In such a case, the system cannot converge to the desired equilibrium point since this becomes unstable. It is therefore important to mitigate such destabilizing effects for making the DBSs implementable in practical applications[7].

Because of such nonlinearity and incremental negative impedance effects of constant power loads (CPLs), over the past decades several nonlinear stabilizing control concepts and compensation techniques have been proposed[10,11,12,13]. In most of the cases, compensation techniques are achieved by adding an extra element; like, passive elements or devices to the power

system or, redesigning the control loop of the source or load converters — also known as active damping [14]. The compensations of CPLs by active damping are normally applied at the DC bus itself or through some auxiliary DC-DC converters system and thus it is only applicable to the cases when feeder of CPL is a switched converter system. Nevertheless, active compensation at the load subsystems levels has also some major disadvantages such as the compensation loop may interfere with main control loop and it may degrade the load performances drastically. Although such a limitation can be easily solved by introducing an auxiliary DC-DC converter between DC bus and load subsystems [15]; it would, however, increase the overall size, weight, cost, and complexity of the system. Moreover, the presence of CPLs reduces effective damping of the system leading to the instability of the whole system and results in significant challenges in its operation and control.

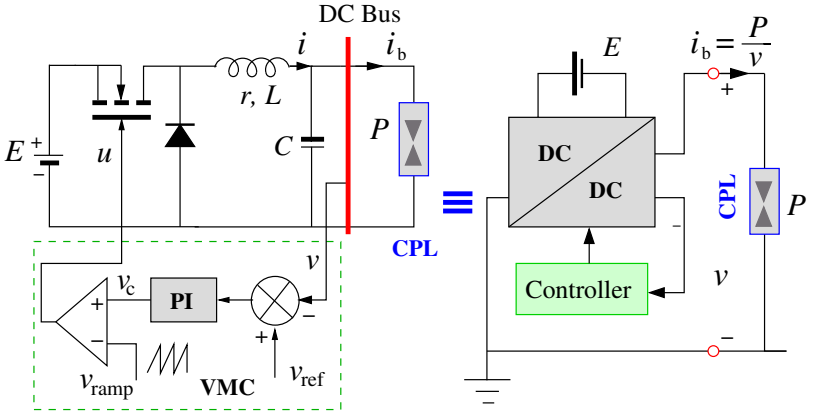

FIGURE 1 A representative buck-type stand-alone DBS with equivalent source voltage E and CPL P.

With these views, this paper explores the cause of occurrence of low frequency LCOs and their suppression in coupled closed-loop DBSs without using any additional hardwares or control circuitries. It has been shown that stabilizing problems of such a nonlinear system can be successfully analyzed by using the concepts of nonlinear dynamics and bifurcation theory, in particular, the amplitude death (AD) phenomena [16,17,18]. An AD is a phenomenon of a nonlinear system by which the desired equilibrium point of interconnected oscillatory systems, or networks, can be stabilized by different types of couplings [17]. There are mainly two reasons which can cause the cessation of LCOs: the strong coupling and the existence of sufficiently different natural frequencies of interaction between the networks [19]. Recently, the coupled DBSs was analyzed by Huddy and Skufca [20] using the concepts of nonlinear dynamics and synchronization of two interconnected open-loop only switched converters without dealing with the cause of occurrence of LCOs. In contrast, this paper explores causes of LCOs and shows that the suppression of such undesired LCOs in two different DBSs is possible through AD phenomena by a suitable heterogeneous coupling between the two systems and that can be used for stabilizing the closed-loop DBSs under this coupling. If heterogeneity — e.g., the system parameters of the source converters are mismatched — are introduced into the systems, the AD can happen by incorporating a small resistance between two or more of DBSs. Such a consideration is quite logical when internal resistances of the connecting wires between several coupled DBSs or parallel power source converters in DC microgrids are considered. Based on these concepts, parameters-space region over which coupled system will be stable can be easily located.

Moreover, it is important to note that heterogeneity of interacting systems plays an important role in the diversity and organization in many complex DC bus systems. Heterogeneity can arise from the nature of connectivity among the systems. The present paper also studies the onset and characterization of interesting collective dynamics or AD phenomena in a network of connected DBSs with differing natural frequency of oscillations. Thus, the heterogeneity induced AD technique that we introduce is different from earlier studies where ineterconnected DBSs with delay feedback controller structures are considered [18]. By considering the relay type complex DC bus network, we study here the effect heterogeneity in the network that can lead to the collective AD behavior.

This paper is organized as follows. Section 2 discusses the dynamic properties of a closed-loop buck-type DBS and its large-signal stability around the desired equilibrium point. Based on this discussion, the cause of instabilities in DBS is analyzed in Section 3. In particular, this section explores how the method of analysis can provide an efficient open-loop control solution

for stabilizing the coupled DBSs and many other complex relay types (or star) networks with linear resistive/diffusive coupling. Finally, stabilizations are numerically assessed and confirmed experimentally for coupled DBSs in Section 4.

2 | BUCK-DERIVED LINE CONDITIONER

Let us consider now the DBS system as shown in Fig. 1. It consists of, for example, voltage-mode controlled buck converter with output low-pass filter inductor with inductance L, capacitor with capacitance C, and parasitic resistance r, respectively; and feeds the power from equivalent input source E to the output CPL P. The role of this switched converter is to maintain the regulated DC voltage across the intermediate bus under slowly varying CPL.

2.1 | Averaged Model and Stability Assessment

In order to ensure this, the linear stability analysis of the stand-alone DBS is performed here. Using a classical averaging technique, the considered DBS can be mathematically described as

$$\frac{dx_1}{dt} = -\frac{rx_1}{L} - \frac{x_2}{L} + \frac{E}{L}d \tag{1}$$

$$\frac{dx_2}{dt} = \frac{x_1}{C} - \frac{P}{Cx_2} \tag{2}$$

with proportional-integral (PI) control algorithm, the variable d is the equivalent continuous control input representing the duty ratio of the square wave driving signal of the power switch and it can be expressed as follows

$$d = k_p(V_{\text{ref}} - x_2) + k_i x_3 \tag{3}$$

where $x = [i\ v\ x_3]^T$, $x_3 = \int_0^t \left(V_{\text{ref}} - x_2\right) dt$ and k_p and k_i are the gains of the PI controller. The duty ratio d is generated by first obtaining an error voltage $v_e = (V_{\text{ref}} - v)$ between the output capacitor voltage v and the reference signal V_{ref} and then processing it by the PI controller to generate a control signal v_c. This signal is further compared with an externally generated sawtooth voltage v_{ramp} with time period T and unity peak-to-peak amplitude to determine the driving signal u for the power switch. Under averaging considerations, the driving signal is approximated by its duty cycle d and the DBS, operating in continuous conduction mode (CCM), can be expressed as a third-order nonlinear differential equation given by

$$\frac{dx}{dt} := F_c(x) = \begin{pmatrix} -\dfrac{rx_1}{L} - \dfrac{x_2}{L} + \dfrac{E}{L}d \\ \dfrac{x_1}{C} - \dfrac{P}{Cx_2} \\ V_{\text{ref}} - x_2 \end{pmatrix}. \tag{4}$$

Nevertheless, considering the output variable of the system is the capacitor voltage, this is a non-minimum phase system[21] and the nonlinearity is due to the term P/x_2. The dynamic behavior of converters loaded by CPLs is thus heavily different from the behavior of converters loaded by other conventional resistive loads or other linear either reactive or capacitive loads.

In order to investigate that, the eigenvalues analysis of proposed DBS is performed here by locally linearizing the system (4) around its equilibrium point, $X_c = [P/V_{\text{ref}} \quad V_{\text{ref}} \quad rP/EV_{\text{ref}} + V_{\text{ref}}/k_i E]^T$. For practical applications, we consider that $x_1 \cong P/V_{\text{ref}}$ and $x_2 \cong V_{\text{ref}}$ are the only useful equilibrium point of the plant. Therefore, to define the local performance of the system the controller parameters k_p and k_i can be easily calculated by simply evaluating the eigenvalues λ_n (for $n = 1, 2, 3$) of Jacobian matrix

$$\mathbf{J_c} = \left(\begin{matrix} -\dfrac{r}{L} & -\dfrac{(k_p E + 1)}{L} & \dfrac{k_i E}{L} \\ \dfrac{1}{C} & \dfrac{P}{Cx_2^2} & 0 \\ 0 & -1 & 0 \end{matrix} \right)\Bigg|_{x = X_c} \tag{5}$$

TABLE 1 System specification under nominal operating condition

Source Converter	Controller and CPL
$r = 0.2\ \Omega$, $L = 72\ \mu$H, $C = 140\ \mu$F,	$k_p = 0.1$, $k_i = 1$,
$V_{\text{in}} = 24.0$ V, $V_{\text{ref}} = 12.0$ V	$f_s = 180$ kHz, $P = 50$ W

whose characteristic polynomial equation is as follows

$$P(\lambda) := \lambda^3 + a_2\lambda^2 + a_1\lambda + a_0 = 0. \tag{6}$$

where $a_2 = \dfrac{r}{L} - \dfrac{P}{CV_{\text{ref}}^2}$, $a_1 = \dfrac{1}{LC}\left(k_pE + 1 - \dfrac{rP}{V_{\text{ref}}^2}\right)$, and $a_0 = \dfrac{k_iE}{LC}$. Note that, the system (4) is stable if the polynomial $P(\lambda)$ has all the roots in the open left-half plane if and only if a_2, a_1 and a_0 are positive and $a_1a_2 > a_0$. Based on these aforementioned criteria, the desired region in the parameter space within which the system is stable is

$$\Pi^r : P < \frac{rCV_{\text{ref}}^2}{L};\ \ \Pi^p : k_p > \frac{1}{E}\left(\frac{rP}{V_{\text{ref}}^2} - 1\right) \tag{7}$$

$$\Pi^i : k_i < \left(k_p + \frac{1}{E} - \frac{rP}{EV_{\text{ref}}^2}\right)\left(\frac{r}{L} - \frac{P}{CV_{\text{ref}}^2}\right). \tag{8}$$

Here, L, C, and V_{ref} are the known circuit parameters and their exact values can be directly substituted into the inequalities (7)-(8) for inspection. However, for a range of E and P, or even unknown parasitic resistance r, it is necessary to consider the boundary points of these parameters values. The confirmation of either the minimum or maximum point of these parameters values is generally sufficient for ensuring the stability condition for the entire range of operation. Knowing the boundary points of r, E and P, it is possible to calculate the boundaries of controller gains k_p and k_i, respectively.

2.2 | Gain Scheduling

Here, the requirement of placing an upper bound on the integral gain $k_i^{\max}$ is obtained by placing the same lower bound requirement on proportional gain $k_p^{\min}$ when condition Π^r is satisfied. While the requirements of k_p is obtained from the condition (7). The closer-look on the stability condition Π^p, however, reveals that proportional gain k_p is always negative for the desired range of E, P and r, respectively; and a smaller positive value of k_p tends to produce larger regions of convergence, suggesting the consideration of the $k_p \to 0$ (but not equal to zero) may be again useful for a practical design process. For example, if we choose $k_p^{\min} = 0.1$, the upper bound on k_i can be expressed as

$$\Pi^i_{\max} := k_i^{\max} = \left(k_p^{\min} + \frac{1}{E} - \frac{rP}{EV_{\text{ref}}^2}\right)\left(\frac{r}{L} - \frac{P}{CV_{\text{ref}}^2}\right). \tag{9}$$

From (9), it can be further observed that the upper bound of integral gain $k_i^{\max}$ is larger for decreased values of r and increased values of P than that of the source voltage variation. Thus, by satisfying the plant stability condition in (7), if one wants to choose the desired PI compensator gain (i.e., $k_i < k_i^{\max}$) over a wide range of load power, the maximum load power $P^{\max}$ and minimum parasitics resistance $r^{\min}$ should be used. Based on the previous parametric constraints, the system is numerically simulated using the parameter values shown in Table 1 except r and k_i. The parameter k_i is then chosen by fulfilling the constraint in (8). For instance, the stability region Π^r in terms of the power P and the resistance r and the stability boundary $\Pi^i_{\max}$ in terms of the power P and the integral gain k_i are depicted in Fig. 2. Note that if all these conditions are simultaneously satisfied, the system will be asymptotically stable. The designer will only have to ensure that the external load power with uncertain parasitic (or series resistive) element r will always remain within the bounded region of the parameter-space Π^r; thereafter, have to choose the controller gain k_i such that $k_i < \Pi^i_{\max} := k_i^{\max}$.

However, this will only provide an intuitive way to choose the controller gains for successful converter operation if bounds of all parameters are known, but does not guarantee its robustness when parameters like load power and circuit parasitic parameters fluctuate. Even, the problem becomes much more complex when two or more DBSs are interconnected. There have been,

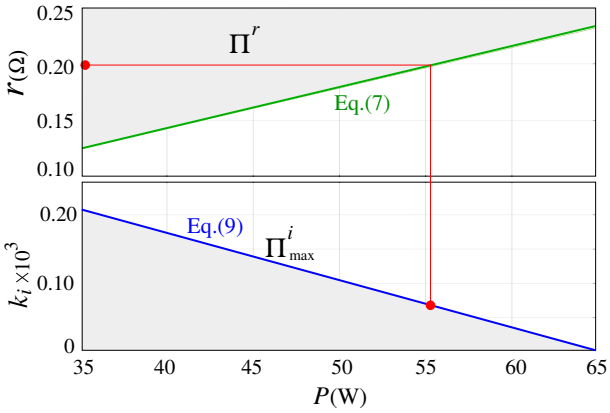

FIGURE 2 Region of Π^r and corresponding zone of integral gain $\Pi^i_{\max}$ for 35 W $\leq P \leq$ 65 W. For a stable DBS operation parameters must satisfy $r \geq \Pi^r$ and $k_i < \Pi^i_{\max}$. The red line denotes the required gain $k_i < k_i^{\max}$ for $r = 0.2\ \Omega$ and $P \approx 55.25$ W.

however, numerous control techniques proposed for the design of isolated DBSs; such as nonlinear feedback linearization and geometrical boundary control, and so on (see[9,11,13,22] and refs. therein). Some of the approaches, such as those found in[8,23], consider the CPL in parallel with a resistive load which compensates the destabilizing effect of the CPL but does often not deliver a feasible mitigation strategy for stabilizing large-scale interconnected DBSs.

3 | CAUSE OF INSTABILITY AND STEADY-STATE BEHAVIOR

Therefore, to identify the stable operating region of the coupled DBSs and to observe their stability status in a slow time-scale, it is necessary to apply the concept of large-scale nonlinear system analysis. It is also necessary to calculate the range of external circuit parameters that will ensure a stable mode of operation in terms of slow-scale dynamical oscillation of the coupled systems. The bifurcation analysis using discrete-time modeling or map was addressed earlier to predict the nonlinear behaviors of the uncoupled DBSs[24,25]. Although this approach is conceptually simple and very powerful to predict the fast-scale instabilities and onset of chaos, it yields complicated equations for most of the switching powers converters[26,27]. Even, this problem becomes more complex for coupled cascaded converters. Using concepts from nonlinear dynamics and bifurcation theory provides an alternative way for performing the stability analysis of coupled DBSs.

3.1 | Cause of Instability

To deal with such a stability analysis of the coupled DBSs, we will first address the cause of instability of an uncoupled DBS and its steady state behaviors. Here the investigation is performed on the basis of full-order large-signal state-space model of the proposed system (4) by deliberately choosing the controller gains k_p and k_i and variable circuit parameter values within the stable domain such as $k_i = 1$, $r = 0.2\ \Omega$ and $P = 55.25$ W, respectively; while keeping the other parameters values the same as in Table 1. The time domain waveforms of the proposed uncoupled DBS are shown in Fig. 3(a). The inductor current x_1, the output capacitor voltage x_2 and the integral variable x_3 of the closed-loop converter asymptotically converge to their steady-state value $X_c = [4.62 \quad 11.95 \quad 0.49]$ [see window ①] with eigenvalues $\lambda_n = -7.22, -3.49 \pm 1.82 \times 10^4 j$. However, as the value of P is increased, the system undergoes a discontinuous Hopf bifurcation (HB) with a jump in eigenvalues at $P := P_c = 55.5$ W causing the instability of the equilibrium point and leading to low frequency oscillation or LCO. The evaluated eigenvalues just after the bifurcation at $P \approx 55.55$ W , $\lambda_n = -7.22, 4.0 \pm 1.82 \times 10^4 j$, indicate that there is a sudden transition in state trajectory of the system. Subsequently, after the discontinuous Hopf bifurcation occurs, the equilibrium point of the converter under CCM operation becomes unstable and the state trajectory becomes diverging until the inductor current hits the border $\Sigma_{\text{CCM-DCM}} := \Sigma(x) = \{x | x_1 = 0\}$. Once the border $\Sigma_{\text{CCM-DCM}}$ is reached [see window ②], the state trajectory is no longer diverging and tends to the equilibrium point $X_d = (P/V_{\text{ref}}, V_{\text{ref}}, V_{\text{ref}}/E)$ of the system under DCM operation which is stable. However, before the equilibrium point is reached, CCM conditions are fulfilled and the converter switches to the CCM operation. This hybrid operation mode leads the system system to exhibit a sustained steady-state oscillation. The steady-state behavior

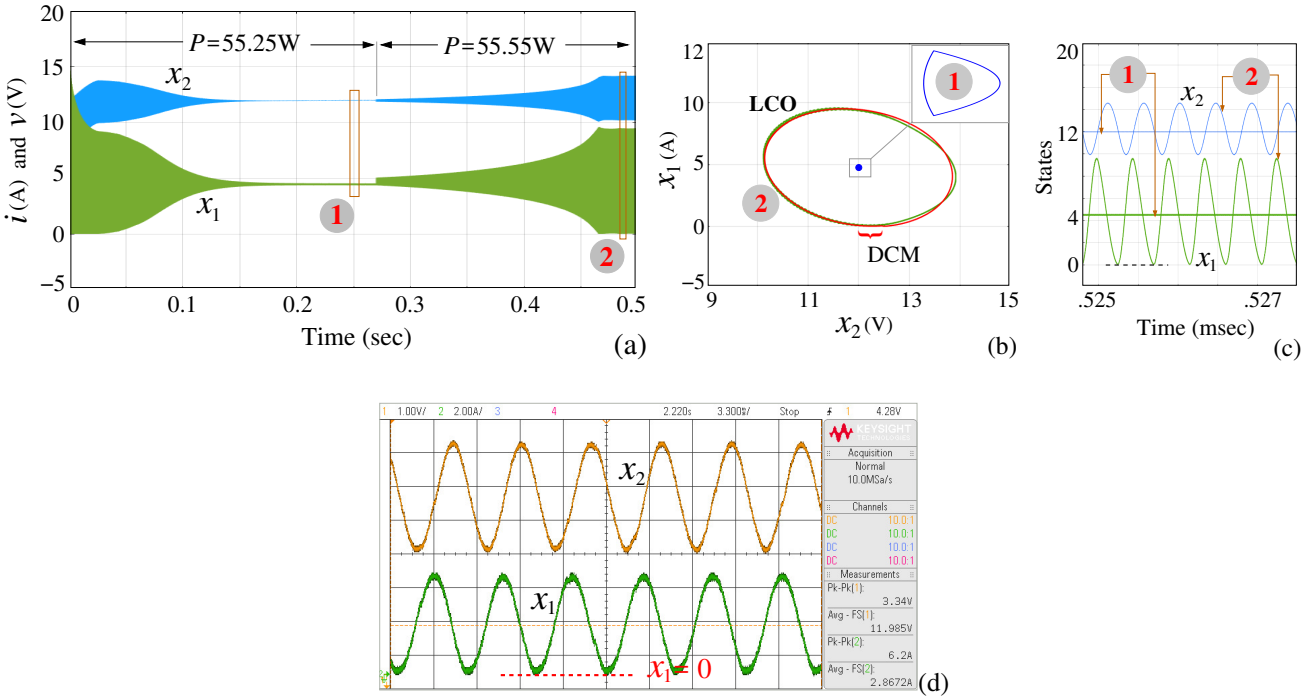

FIGURE 3 The representative trajectory evolutions showing different dynamical behaviors under power variation. (a) Time-domain waveforms indicating the transition from a stable steady-state equilibrium point to stable LCO. (b) and (c) Close-up views of state-plan trajectory and time-domain waveforms at ① and ②, respectively. (d) Experimental validation of (c).

(in terms of state-plane trajectory and time-domain waveforms) are shown in Fig. 3(b)-(c), respectively. Their corresponding experimental time-domain waveforms are shown in Fig. 3(d).

Under this steady-state regime characterized by sustained oscillation, the dynamics of the closed-loop system is governed by averaged dynamics of both CCM and DCM operation modes with interacting switching surface $\Sigma_{\text{CCM-DCM}}$. Let Σ_{CCM} the region in the state space where the DBS operates in CCM and let Σ_{DCM} where it is under DCM operation. The dynamics of the DBS in Σ_{CCM} is governed by (4) while in Σ_{DCM} it is given by[28]

$$\frac{dx}{dt} := F_d(x) = \begin{pmatrix} -\dfrac{rx_1}{L} - \dfrac{2x_1x_2f_s}{d(E-x_2)} + \dfrac{E}{L}d \\ \dfrac{x_1}{C} - \dfrac{P}{Cx_2} \\ V_{\text{ref}} - x_2 \end{pmatrix} \tag{10}$$

where $f_s = 1/T$ is the switching frequency of the converter. Therefore, to understand the occurrence of Discontinuity Induced HB (DIHB) and how it differs from the classical smooth HB, one has to evaluate the stability status of the complete one-cycle LCO using eigenvalues analysis.

3.2 | Analysis using Generalized Jacobian Matrix

From a dynamical system point of view, the DBS can be described by a 3-dimensional (3-D) set of differential equations with discontinuous right-hand side as

$$\frac{dx}{dt} = \begin{cases} F_c(x) \;\; x \in \Sigma_{\text{CCM}} & \text{if } \Sigma(x) > 0 \\ F_d(x) \;\; x \in \Sigma_{\text{DCM}} & \text{if } \Sigma(x) \leq 0 \end{cases} \tag{11}$$

where $\Sigma(x) = 0$ is the discontinuous switching surface partitions the state-space region into two smooth compartments: Σ_{CCM} and Σ_{DCM}. Note that the switching system (11) is called continuous if $F_c(x) = F_d(x)$ at any point of the boundary between these adjacent regions Σ_{CCM} and Σ_{DCM}. The vector field is also uniquely defined at any point of the state space if trajectory,

say, in $\Sigma_{\rm CCM}$ approaching transversally the boundary and crosses it, and then enters into the adjacent $\Sigma_{\rm DCM}$. If the transversal components of $F_c(x)$ and $F_d(x)$ are of opposite sign, i.e., if the two vector fields are pushing in opposite directions, the state of the system is forced to remain on the boundary and slide on it[26]. On the contrary, if the transversal components of $F_c(x)$ and $F_d(x)$ have the same sign, the trajectory crosses the boundary and has at that point a discontinuity in its tangent vector. The overall behavior is affected by the vector fields on both sides of the switching boundary and the combined effect can lead to the birth of LCOs, including creation and destruction of boundary equilibrium bifurcation[29]. Here in the DBS, as boundary equilibrium bifurcations are not observed, it is found that perturbing the boundary equilibrium point in $\Sigma_{\rm CCM}$ results in the trajectory forming a limit-cycle attractor.

Usually, the bifurcation analysis associated with the equilibrium point of the smooth system is investigated by classical Jacobian matrix evaluated at that point. However, due to lack of smoothness in vector field, the calculation of Jacobian matrix of nonsmooth system cannot be same as for smooth dynamical system. One can employ the concept of generalized differential equation to deduce the so-called generalized Jacobian matrix of nonsmooth DBS near the switching surface discontinuity $\Sigma(x) = 0$[29,30]. Here we found that, during transition, trajectory evolution from $\Sigma_{\rm CCM}$ to $\Sigma_{\rm DCM}$ does not occur transversely at switching surface $\Sigma(x)$, rather it travels along $\Sigma(x)$ for a short duration of time. The vector field $F_c(x)$ remains continuous until it reaches the boundary. Once it hits the boundary, it bounces back and follows the DCM dynamics $\dot{x} = F_d(x)$ to smoothly return into the region $\Sigma_{\rm CCM}$. As a result, one can overcome the problem of single discontinuity with a set-valued function $F(x)$ as[31]

$$\frac{dx}{dt} := F(x) = \overline{\rm co}\left\{F_c(x), F_d(x)\right\} \qquad x \in \Sigma_{\rm CCM-DCM} \tag{12}$$

where the symbol $\overline{\rm co}\left\{F_c(x), F_d(x)\right\}$ denotes the smallest closed convex set containing $F_c(x)$ and $F_d(x)$. This convex set with two piecewise-smooth functions (PWS) $F_c(x)$ and $F_d(x)$ can be then represented as $\overline{\rm co}\{F_c(x), F_d(x)\} = (1-q)F_c(x) + qF_d(x)$, and a scalar function

$$q = \frac{\nabla\Sigma(x)F_c(x)}{\nabla\Sigma(x)\left[F_c(x) - F_d(x)\right]} \quad \text{and} \quad 1-q = \frac{-\nabla\Sigma(x)F_d(x)}{\nabla\Sigma(x)\left[F_c(x) - F_d(x)\right]} \quad \forall q \in (0,1). \tag{13}$$

Here, the system (12) with Fillipov coefficient (13) represents the equivalent flow inside the region $\Sigma_{\rm CCM-DCM}$. It describes the average dynamics of the impinging vector fields $F_c(s)$ and $F_d(s)$ weighted by the proportion of their time-flow spent in each mode. Thus, to ensure the continuity condition near the switching instant, the trajectories as a set must be tangent to the switching surface[32]. This can only happen when the long-time averaged value of the coefficient q becomes constant[32,33]. This coefficient is known as the Fillipov coefficient. Once this coefficient is well defined, there will not be any transversal component of the average vector field $F(x) \in (F_c(x), F_d(x))$ along the discontinuity surface. Using (4), (10) and (13), one can derive this transversal condition as $\nabla\Sigma(x)F(x) = 0$, and from it, can evaluate the required Fillipov coefficient q as

$$q|_{X=X_\Sigma} := \left.\frac{-\dfrac{rx_1}{L} - \dfrac{x_2}{L} + \dfrac{E}{L}d}{-\dfrac{x_2}{L} + \dfrac{2x_1x_2f_s}{d(E-x_2)}}\right|_{X=X_\Sigma} = 1 - \frac{dE}{V_{\rm ref}} \tag{14}$$

where $X_\Sigma = (0, V_{\rm ref}, V_{\rm ref}/E)$ is the value of state vector near the switching boundary. Note that this coefficient q is unique and solution of (12) is an absolutely continuous vector-valued function. Before the transition it satisfies (11), and after the transition it satisfies $\dot{x} = F(x)$ for almost all $t \to \infty$. Thus, the problem of discontinuity can be overcome with a set-valued function $F(x)$ and it is possible to know the system behavior near switching discontinuity by setting up a generalized Jacobian matrix J_q at the equilibrium point X_c[29,30]. This generalized Jacobian matrix is a set-valued matrix and is given as

$$\mathbf{J}_q = (1-q)\mathbf{J}_c + q\mathbf{J}_d \quad \forall \quad q \in [0,1] \tag{15}$$

where $\mathbf{J}_c$ is the known Jacobian matrix for CCM. While Jacobian matrix for DCM operation $\mathbf{J}_d$ can be evaluated, from (10) and (3), as

$$\mathbf{J}_d = \left.\begin{pmatrix} \alpha & \beta & \gamma \\ \dfrac{1}{C} & \dfrac{P}{Cx_2^2} & 0 \\ 0 & -1 & 0 \end{pmatrix}\right|_{x=X_c} \tag{16}$$

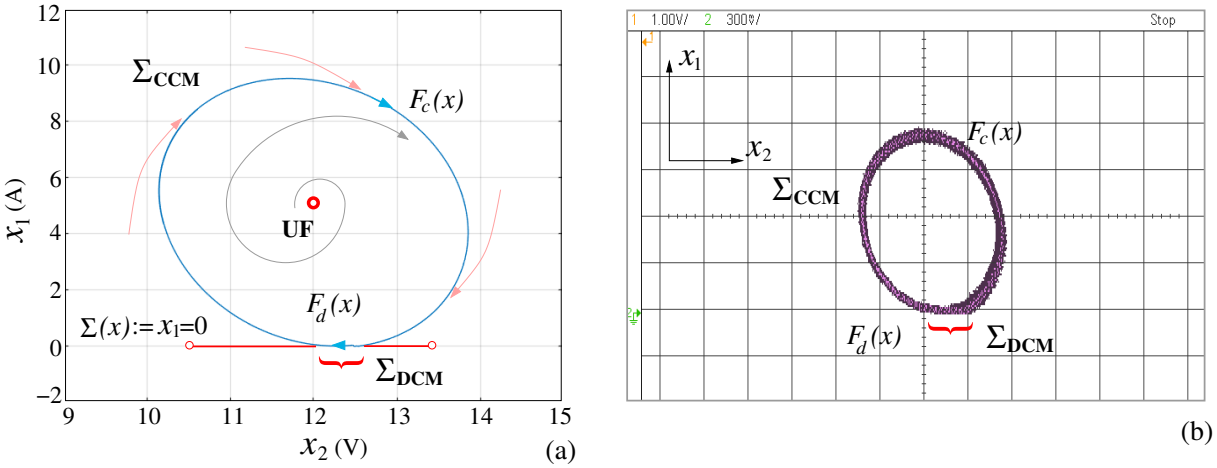

FIGURE 4 State plane trajectory showing the transition from unstable focus (**UF**) to stable LCO through DIHB. (a) Simulation result. (b) Experimental confirmation.

$$\text{where } \alpha = -\frac{r}{L} - \frac{2V_{\text{ref}} f_s}{d(E - V_{\text{ref}})},\ \beta = -\frac{k_p E}{L} - \frac{2P f_s}{dV_{\text{ref}}(E - V_{\text{ref}})}\left(\frac{E}{E - V_{\text{ref}}} + \frac{k_p V_{\text{ref}}}{d}\right),\ \text{and}\ \gamma = \frac{k_i E}{L} + \frac{2P f_s}{d^2(E - V_{\text{ref}})}.$$

3.3 | Discontinuity-Induced Hopf Bifurcation

To explore the cause of this DIHB, we numerically calculate the Jacobian matrices of Clarke's generalized differential to obtain the differential equation $\dot{x} = F(x)$, and then its generalized Jacobian matrix and the corresponding eigenvalues. Because the vector field is nonsmooth but still continuous, the generalized differential of Clarke is used to set up a generalized Jacobian matrix [30,29]. The evolution of nonsmooth dynamics near the switching discontinuities is investigated by setting up a generalized Jacobian matrix J_q just after the transition from CCM, say, at $P = 55.55$ W . This generalized Jacobian matrix is a set-valued matrix and is given by (15). The dynamics in the vicinity of the equilibrium for $\rho < 0$ (where $\rho = P - P_c$) is therefore determined by the Jacobian matrix $\mathbf{J}_c$ with eigenvalues λ_n^c, and for $\rho > 0$ by the Jacobian matrix $\mathbf{J}_d$ with eigenvalues λ_n^d, as given in (17).

$$\mathbf{J}_c := \begin{pmatrix} -\frac{r}{L} & -\frac{(k_p E + 1)}{L} & \frac{k_i E}{L} \\ \frac{1}{C} & \frac{P}{CV_{\text{ref}}^2} & 0 \\ 0 & -1 & 0 \end{pmatrix} = 10^5 \times \begin{pmatrix} -0.02778 & -0.4722 & 3.3333 \\ 0.07142 & 0.02826 & 0 \\ 0 & -0.00001 & 0 \end{pmatrix};\ \lambda_n^c = \begin{cases} -7.227 \\ 27.7651 \pm 1.8151 \times 10^4 j \end{cases} \quad \text{for } \rho < 0$$

$$\mathbf{J}_d := \begin{pmatrix} \alpha & \beta & \gamma \\ \frac{1}{C} & \frac{P}{CV_{\text{ref}}^2} & 0 \\ 0 & -1 & 0 \end{pmatrix} = 10^5 \times \begin{pmatrix} -12.44372 & -7.31375 & 73.66523 \\ 0.07142 & 0.02826 & 0 \\ 0 & -0.00001 & 0 \end{pmatrix};\ \lambda_n^d = \begin{cases} -1.240 \times 10^6 \\ -1.345 \times 10^3, -31.540 \end{cases} \quad \text{for } \rho > 0 \qquad (17)$$

Looking at the eigenvalues just before and after the bifurcation point $P_c = 55.5$ W (see Figs. 3 and Fig. 4), it is seen that the equilibrium is an unstable focus for $\rho < 0$ and a stable node for $\rho > 0$, if it is solely governed by $\dot{x} = F_d(x)$ dynamics. Moreover, it is important to note that when the auxiliary variable $q = 0$, then from (15) we find that $\mathbf{J}_q = \mathbf{J}_c$. In this case, the eigenvalues λ_n^q reduce to the eigenvalues of the Jacobian matrices $\mathbf{J}_c$ in the CCM region. While for $q = 1$ we find that $\mathbf{J}_q = \mathbf{J}_d$. Hence the eigenvalues λ_n^q reduce to the eigenvalues of the Jacobian matrix $\mathbf{J}_d$ in the DCM region. These are shown by enclosed empty circles in Fig. 5. For other intermediate values of the auxiliary variable q, the eigenvalues of the generalized Jacobian are set-valued $\lambda_n^q, q \in [0, 1]$ and form a one-dimensional (1-D) path in the complex s-plane. Following this 1-D path, we find that the eigenvalues become purely imaginary, i.e., $\lambda_n^q = \pm \approx 1.815 \times 10^4 j$ at $q \approx 0.001$. These generalized eigenvalues λ_n^q are shown

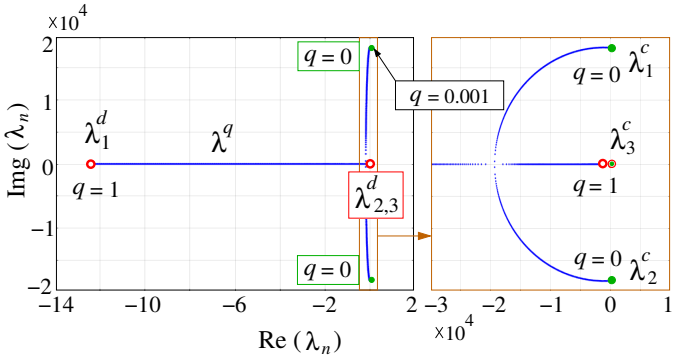

FIGURE 5 Eigenvalues-path representing the DIHB of DBS (15) under the variation of P from 55.25 W to 55.55 W. All other parameters value are the same as in Table 1.

by arrows in Fig. 5 and are found to jump through the imaginary axis as a conjugate pair; thereby, suggesting the occurrence of a DIHB when the discontinuity surface $\Sigma_{\text{CCM-DCM}}$ is reached. Indeed, the existence of this stable discontinuity-induced LCO can also be verified by using the nonsmooth version of Bendixson's criterion[30] according to which if the condition

$$\text{trace}(\mathbf{J}_c)\ \text{trace}(\mathbf{J}_d) < 0 \tag{18}$$

is satisfied, then there exists a stable discontinuity-induced LCO in the nonsmooth dynamical system (see ref.[30] for theorems and proofs). In our case, the previous condition is fulfilled since $\text{trace}(\mathbf{J}_c)\ \text{trace}(\mathbf{J}_d) = -5.997 \times 10^7 < 0$. This bifurcation, though discontinuous, is very similar to continuous HB found in smooth dynamical systems, but not exactly the same as in[25] where a discrete-time approach has been used to predict the onset of bifurcation in DC power electronics-based cascaded systems.

By considering the DBS as an oscillator, the stabilizing problem of coupled oscillatory DBSs can be thus successfully achieved by using the concept of AD phenomena[34].

4 | STABILIZATION OF COUPLED DBS

Oscillation death refers to the phenomena where coupled oscillators stop oscillating and exhibit an equilibrium point in steady-state regime[20]. Ideally, it is a phenomenon whereby two or more autonomous oscillatory systems reach a stable stable equilibrium point when they are coupled. If the equilibrium point corresponds to the unstable equilibrium point of the uncoupled oscillators — occurs just after the coupling, then oscillation death is called as AD; otherwise, it is simply called as the oscillation death[34]. In this paper, it is shown that AD has a very important role in the dynamics of coupled oscillator systems where a set of two nonidentical DBSs are coupled to each other via simple resistive or diffusive coupling. The representative diagram of this diffusively coupled DBSs and their uncoupled mode of oscillations for different inductance values, $L_a = 90\mu$H and $L_b = 72\mu$H, are shown in Fig. 6.

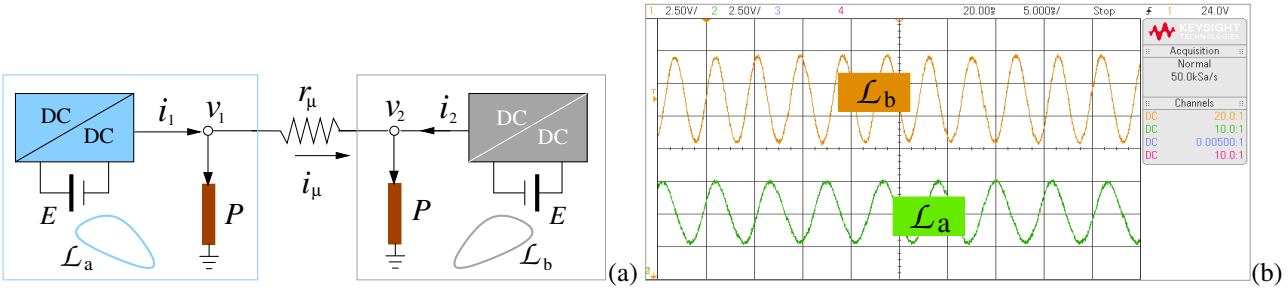

FIGURE 6 (a) Schematic diagram of the diffusively coupled oscillatory DBSs. (b) Oscillatory bus voltages for $L_a = 90\mu$H and $L_b = 72\mu$H.

4.1 | Diffusive Coupling Between Identical DBSs

In order to begin with such a coupling effect, let us first consider the identical DBSs (as oscillators) which are diffusively coupled through a simple series resistance r_μ. As a result, current through the coupling resistance is given by $i_\mu = (v_1 - v_2)/r_\mu$, where v_1 and v_2 are the capacitor voltages of the oscillators $\mathcal{L}_a$ and $\mathcal{L}_b$, respectively. It is also assumed that near a DIHB each of these oscillators is governed by an approximate generalized differential equation (12) with $q := .001 \approx 0$, and dynamics of diffusively coupled DBSs thus can be described by equations

$$\begin{aligned} \frac{dx_a}{dt} &= F_1(x_a) + \sigma(v_1 - v_2) \\ \frac{dx_b}{dt} &= F_2(x_b) + \sigma(v_2 - v_1) \end{aligned} \tag{19}$$

for two different oscillators F_1 and F_2, where x_a is the vector of the state variables for the first DBS and x_b the one corresponding to the second DBS, with common scalar coupling coefficient $\sigma = 1/r_\mu$. If F_1 and F_2 are identical, i.e., all the parameters of two DBSs are equal, then diffusive coupling does not cause the DBSs to stop oscillating and to stabilize at the desired steady-state equilibrium point. Such an obvious statement can be easily proved by examining eigenvalues of the Jacobian matrix $\mathbf{J}$ of the coupled DBSs (19) which is given by

$$\mathbf{J} = \begin{pmatrix} \mathbf{A}_a & \mathbf{B} \\ \mathbf{B} & \mathbf{A}_b \end{pmatrix} \tag{20}$$

where $\mathbf{A}_a$, $\mathbf{A}_b$ and $\mathbf{B}$ are given by

$$\mathbf{A}_a = \mathbf{A}_b = \begin{bmatrix} -\frac{r}{L} & -\frac{(k_p+1)}{L} & \frac{k_i E}{L} \\ \frac{1}{C} & \frac{1}{C}\left(\frac{P}{V_{\text{ref}}^2} - \sigma\right) & 0 \\ 0 & -1 & 0 \end{bmatrix} \quad \text{and} \quad \mathbf{B} = \begin{pmatrix} 0 & 0 & 0 \\ 0 & \frac{\sigma}{C} & 0 \\ 0 & 0 & 0 \end{pmatrix}$$

Now, using the properties of symmetric block-diagonal matrix and the coefficients a_0, a_1, a_3 used in Section 2.1, we obtain the set of characteristic polynomial equations of both DBSs:

$$P(\lambda) := \begin{cases} \lambda^3 + a_2\lambda^2 + a_1\lambda + a_0 = 0 \\ \lambda^3 + \left(a_2 + \frac{2\sigma}{C}\right)\lambda^2 + \left(a_1 + \frac{2r\sigma}{LC}\right)\lambda + a_0 \end{cases} \tag{21}$$

whose eigenvalues λ_n yields the stability condition of the desired equilibrium point:

$$P < \frac{rCV_{\text{ref}}^2}{L} \quad \text{and} \quad \sigma > \frac{P}{2V_{\text{ref}}^2} - \frac{rC}{2L}. \tag{22}$$

If the conditions in (22) are simultaneously satisfied, then the coupled system is stable. However, since near DIHB this condition is violated, (see Fig. 2 in Section 2.2), the equilibrium point is still unstable. Therefore, it can be concluded that linear diffusive coupling of two identical oscillators cannot stabilize the equilibrium point; hence, the coupled system remains unstable and will exhibit sustained LCOs.

4.2 | Stabilization Through Nonidentical Coupled DBSs

An unstable equilibrium point can be successfully stabilized when two or more inhomogeneous (or unmatched) oscillators are mutually coupled. A theoretical analysis was given in [16], which considered a pair of linearly coupled oscillators and each of them is operating close to a HB point. In particular, it was established that for a general class of coupled oscillatory systems AD can happen when oscillators' frequency are sufficiently different and coupling is diffusive. Also, it has been proved that there exists a certain range of coupling coefficient within which the interaction causes the system to stop oscillating and the system stabilized at the desired equilibrium point, iff

$$\Delta\omega \equiv |\omega_a - \omega_b| > \sigma \tag{23}$$

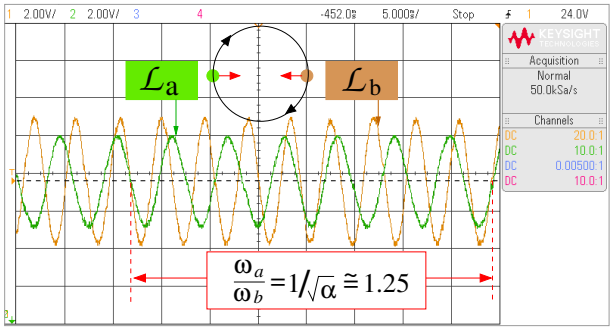

FIGURE 7 Frequency mismatch of the coupled DBSs for $\alpha \approx 0.6$.

is satisfied [16], where ω_a and ω_b are the corresponding oscillation frequencies at their HB points. With these views, the inductance value of each DBS is set as before in order to achieve AD under resistive/diffusive coupling. This is because the equilibrium point of the system does not depend on the inductance value and changing its value changes the oscillation frequency. The oscillation frequencies of the two uncoupled DBSs and their correlation are illustrated in Fig. 7. The waveforms in this figure were obtained from experimental measurements. The circle indicates the periodic oscillation of the uncoupled LCOs ($\mathcal{L}_a$ and $\mathcal{L}_b$, respectively) whose oscillation angular frequencies are approximately given by:

$$\frac{\omega_a}{\omega_b} \approx \sqrt{\frac{L_b}{L_a}} = \frac{1}{\sqrt{\alpha}}$$

where $\alpha = L_a/L_b$ is the heterogeneity factor. Note that, for different oscillation periods, two oscillators will not be at the same point of the cyclic orbit. The arrows on the circle show the traveling directions of the oscillators and two inward pointing arrows shows the interaction between the two oscillators due to coupling. This coupling results in the two oscillators to pull each other off from their uncoupled periodic orbits and brings the overall system to collapse to an equilibrium point under a certain range of σ and α.

4.2.1 | Dynamics of Two Coupled DBSs

To illustrate this idea, the numerical simulation of the coupled DBSs is first performed and then the results are confirmed experimentally by using the parameters set $\alpha = 0.6$ and $\sigma = 1/r_\mu = 4.0$ ℧. Fig. 8 shows the dynamical behavior of the coupled DBSs. First the coupling is disabled and it is connected at $t = 10$ ms. Thereore, each DBS without coupling ($\sigma = 0$) before $t = 10$ ms, exhibits LCO. When the resistive coupling is applied at $t = 10$ ms, the oscillations vanish after an initial transient time interval, t_s, and the coupled system trajectory finally converges to a steady-state equilibrium.

However, in order to obtain the guaranteed nominal stable mode of operation or AD region, it is necessary to calculate the range of variable parameters within which the equilibrium point of the DBSs is stable. It is also necessary to calculate the required coupling resistance value for minimum power loss. The bifurcation diagram in Fig. 9 shows such a desired mode of stable operation over the parameter-space $r_\mu - \alpha$: $0.1\ \Omega \leq r_\mu = 1/\sigma \leq 10\ \Omega$, $0.01 \leq \alpha \leq 1$for $0.1\ \Omega \leq r_\mu = 1/\sigma \leq 10\ \Omega$ and $0.01 \leq \alpha \leq 1$. The results show that regardless the value of the coupling resistance r_μ, coupled DBSs always exhibit a sustained oscillation for higher values of heterogeneity factor $\alpha > 0.95$. However, for lower values of α, the system is stabilized to a an equilibrium point within for $0.1\ \Omega \leq r_\mu \leq 9.5\ \Omega$. Varying the bifurcation parameters, for example, from inside to outside the stability region leads the system to change its steady-state dynamical behavior from a stable equilibrium point to a stable limit cycle due to an abrupt jump of a pair of complex conjugate eigenvalues from left to right-half side of the s-plane (also see insets of Fig. 9 for the calculated maximum Lyapunov exponent $\lambda_{\max}$). This is a DIHB and it is different from the smooth HB by the fact that at the bifurcation point, the eigenvalues of the system jumps through the imaginary axis in the s-plane. The representative trajectory evolutions showing such transition from stable LCO to AD phenomena accross the different boundary points **A**, **B** and **C** are shown in Fig. 10.

Therefore, one can find that for a sufficiently different natural oscillation frequencies and with a strong coupling strength σ, both oscillators collapse to a desired steady-state equilibrium point under resistive coupling. Such a concept can be further extended for DC bus networks with multiple converters. In real situations, bus systems consist of multiple power sources and loads. For instance, in [18], it was analytically shown that the dynamics of DC networks consisting of several identical DBSs

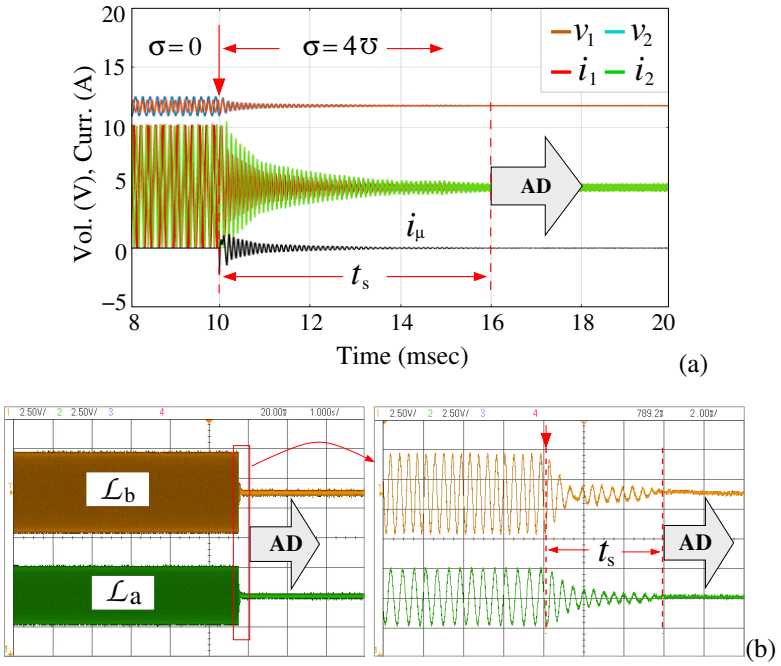

FIGURE 8 Amplitude death of DC bus voltages due to diffusively coupled heterogeneous DBSs for $\alpha = 0.6$ and $\sigma = 4.0\,\mathfrak{V}$. (a) Simulation result. (b) Experimental validation.

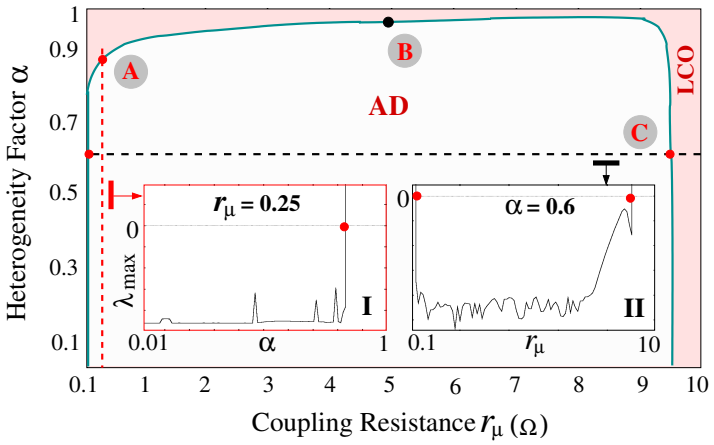

FIGURE 9 Domains of existence for the different dynamical behaviors in the system parameter plane r_μ-α. Insets represent the calculated maximum Lyapunov exponent λ_{max} along the dotted lines, for $r_\mu = 0.25\ \Omega$ and $\alpha = 0.6$.

connected by resistors that the stability can be guaranteed independently of the number of bus systems and the network topology by using delay feedback. In the same paper it was demonstrated that the stabilization of the whole network does not depend on the number of bus systems or the network topology. Applying AD techniques for stabilizing a more practical electrical network in which each DC bus system has different parameters with different converter topologies and controls could be an interesting research topic.

4.2.2 | Collective Behaviour of DC Bus Network

This section, however, deals with the dynamics of a complex DC grid network which is coupled in relay; namely, through an intermediary heterogeneous system. From previous investigations, it has been found that coupled system show a transition from steady-state equilibrium to LCO and vice versa when the interactions involve a time delay [18]. Here we show that, in the absence

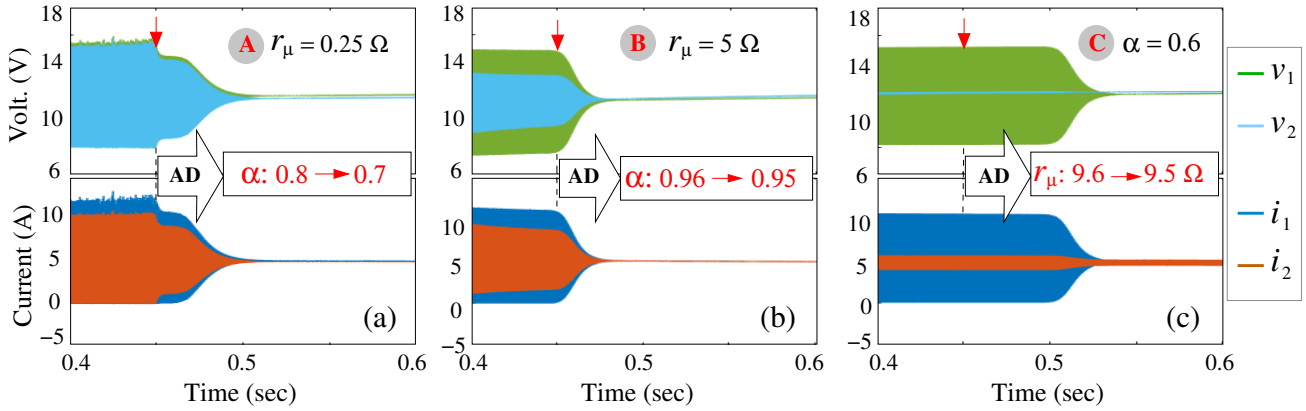

FIGURE 10 Trajectory evolutions showing the transition from stable LCO to steady state equilibrium. (a) α: 0.8 → 0.7, r_μ = 0.25 Ω. (b) α: 0.96 → 0.95, r_μ = 5 Ω. (c) α = 0.6, r_μ: 9.6 Ω → 9.5 Ω.

of time delay, relay coupling through heterogeneous system has the same effect. The purpose of present study is to analyze the onset and characterization of collective AD in a network of connected DBSs with different natural frequency of oscillations. By considering the heterogeneously coupled relay network, we study the effect heterogeneity in a network that can lead to the desired AD behavior.

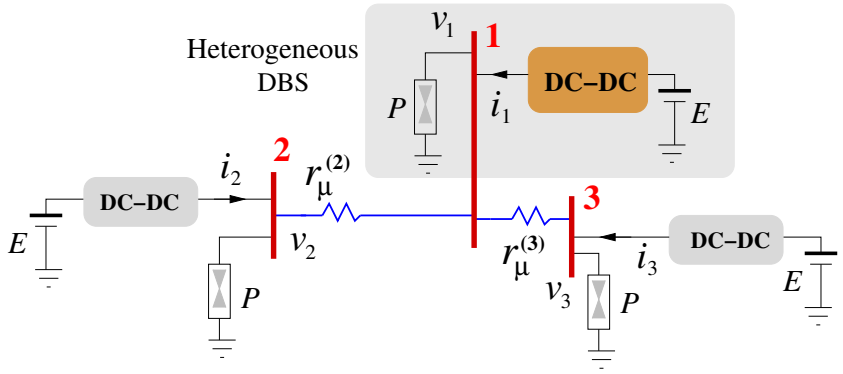

FIGURE 11 A schematic of relay-coupled heterogeneous DC bus network.

In order to unveil the existence of such AD phenomena, let us consider the relay system as shown in Fig. 11 in which second and third systems are coupled only to the first system through a simple resistive link. Here we calculate the range of coupling resistance within which the equilibrium point of the DBSs is stable and draw the largest Lyapunov exponent λ_{max} to estimate the onset of steady state equilibrium as shown in Fig. 12. Note that, when largest Lyapunov exponent λ_{max} is negative, the AD occurs; otherwise, systems exhibit consistent periodic oscillations. For instance, during the oscillation at higher coupling parameters $r_\mu^{(2)} = r_\mu^{(3)} = 10\ \Omega$, two indirectly coupled DBSs have a zero-phase difference and phases of the directly coupled pairs have the same nonzero phase difference [Fig. 13]. Inspection of this system dynamics also reveals that the second and third oscillators are completely synchronized while the middle one has a different amplitude and a r_μ-dependent phase shift compared to its neighbors. However, there is an abrupt transition in the Lyapunov exponent and the corresponding phase difference between any two neighboring oscillators when the coupling resistance passes through the critical value $r_\mu^c = 9.6\ \Omega$. After the transition, the mean phase difference between two neighboring oscillators and their amplitude of oscillations become nearly zero, indicating the partial stabilization. However, below the critical resistance $r_\mu^{(2)} = r_\mu^{(3)} = 5.0\ \Omega < r_\mu^c$, systems go into the anti-phase oscillations leading to complete stabilization or AD behavior as shown in Fig. 13 and its enlarged views. These results thus indicate that, even though the spatial systems are coupled instantaneously, there is an inherent delay in the communication among different indirectly coupled oscillators and makes the system stable .

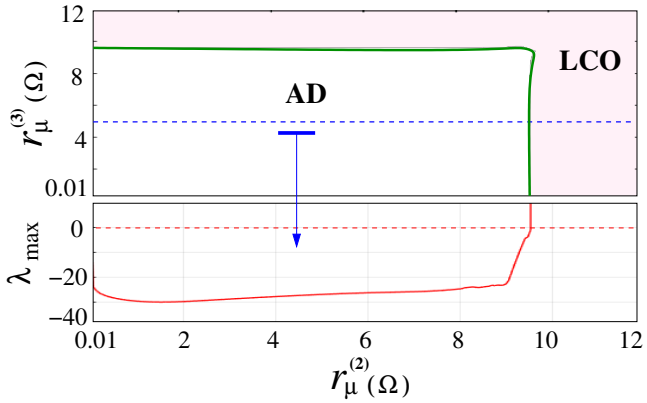

FIGURE 12 Region of AD and LCO in the system parameter plane $r_\mu^{(2)} - r_\mu^{(3)}$ for $\alpha = 0.6$. Bottom trace represents the calculated maximum Lyapunov exponent λ_{max} along the dotted blue line, for $r_\mu^{(3)} = 5.0\ \Omega$.

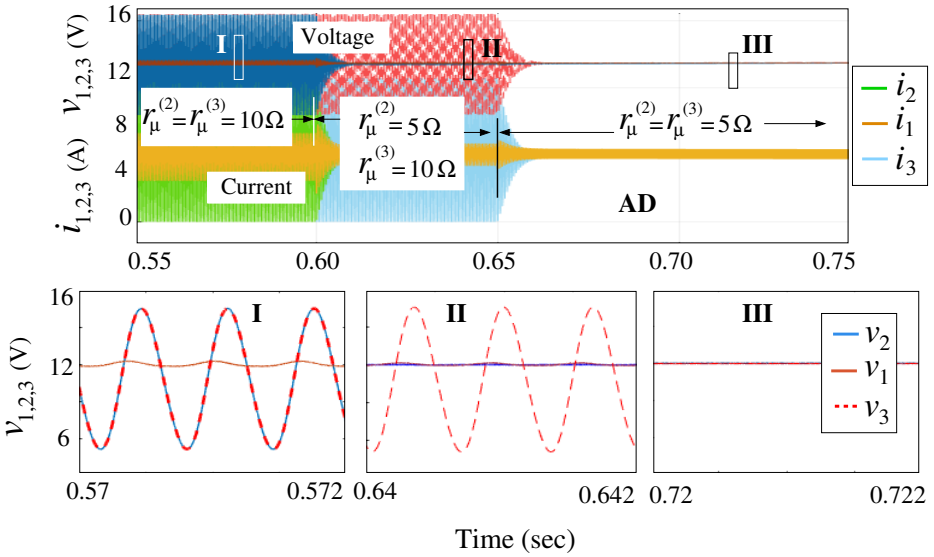

FIGURE 13 Dynamic response of the proposed relay-coupled DBSs as a function of coupling resistance. (I) Complete synchronization or LCO for $r_\mu^{(2)} = r_\mu^{(3)} = 10\ \Omega$; (II) Partial stabilization for $r_\mu^{(2)} = 5\ \Omega$ and $r_\mu^{(3)} = 10\ \Omega$; and (III) Complete stabilization or AD for $r_\mu^{(2)} = r_\mu^{(3)} = 5\ \Omega$.

As a result, the coupling among several distributed systems can give rise to a synchronizing tendency and the interaction through heterogeneous coupling has a tendency to drive the overall system to a state where the sum of the all variables is small. The combined effect of these two tendencies is to lead the coupled systems to the state of AD. This method has thus the advantage that it involves a single damped heterogeneous system coupled to all peripheral converters equally and hence the design procedure is simple and easy to implement. It could be very effective in complex DC networks with star topologies.

5 | CONCLUSION

This papers has addressed the large-signal behavior of the DBSs and has provided a tool that can be used to assess the trade-offs between local regulation and global behaviors under wide parameters variations. It has been shown that CPLs on DPS create a destabilizing effect on the system that can lead to severe voltage oscillations caused by discontinuity-induced HB — which are qualitatively different from the bifurcations known for smooth dynamical systems. Based on this analysis, a stand-alone

DBS is modeled as a nonlinear oscillator and the concepts of AD techniques is applied to stabilize the coupled DBSs of DC grid network. Moreover, this paper has also prposed a simple but efficient resistive coupling technique to retrieve the desired stable steady-state behavior. When the coupling is sufficiently strong and the frequency difference between the two or more uncoupled DBSs are sufficiently large, the overall system undergoes AD phenomenon leading to the stabilization of the coupled system. The region of coupling coefficient and heterogeneity factor, within which AD always persists, has been determined and an experimental validation of such a phenomen on in coupled DBSs has been presented.

References

1. Jovanovic MM, Lee F, others . Present and Future of Distributed Power Systems. In: ; 1992: 161–168.
2. Xu Q, Hu X, Wang P, et al. A decentralized dynamic power sharing strategy for hybrid energy storage system in autonomous DC microgrid. *IEEE Transactions on Industrial Electronics* 2016; 64(7): 5930–5941.
3. Li H, Guo Z, Liu C, Zheng TQ. An extensible stability analysis method in time domain for cascaded DC-DC converters in electrical vehicles. *Microelectronics Reliability* 2018; 88: 1293–1299.
4. Yu J, Yu J, Wang Y, Cao Y, Lu X, Zhao D. Passivity-based active stabilization for DC microgrid applications. *CSEE Journal of Power Energy Systems* 2018; 4(1): 29–38.
5. Kakigano H, Miura Y, Ise T. Low-voltage bipolar-type DC microgrid for super high quality distribution. *IEEE Transactions on Power Electronics* 2010; 25(12): 3066–3075.
6. Kwasinski A, Onwuchekwa CN. Dynamic behavior and stabilization of DC microgrids with instantaneous constant-power loads. *IEEE Transactions on Power Electronics* 2011; 26(3): 822–834.
7. Mohamad AM, Mohamed YARI. Investigation and assessment of stabilization solutions for DC microgrid with dynamic loads. *IEEE Transactions on Smart Grid* 2019; 10(5): 5735–5747.
8. Chang F, Cui X, Wang M, Su W, Huang AQ. Large-signal stability criteria in DC power grids with distributed-controlled converters and constant power loads. *IEEE Transactions on Smart Grid* 2020; 11(6): 5273–5287.
9. Emadi A, Khaligh A, Rivetta CH, Williamson GA. Constant power loads and negative impedance instability in automotive systems: definition, modeling, stability, and control of power electronic converters and motor drives. *IEEE Transactions on Vehicular Technology* 2006; 55(4): 1112–1125.
10. Zhao Y, Qiao W, Ha D. A sliding-mode duty-ratio controller for DC/DC buck converters with constant power loads. *IEEE Transactions on Industry Applications* 2013; 50(2): 1448–1458.
11. Onwuchekwa CN, Kwasinski A. Analysis of boundary control for buck converters with instantaneous constant-power loads. *IEEE Transactions on Power Electronics* 2010; 25(8): 2018–2032.
12. Herrera L, Zhang W, Wang J. Stability analysis and controller design of DC microgrids with constant power loads. *IEEE Transactions on Smart Grid* 2017; 8(2): 881–888.
13. Xu Q, Zhang C, Wen C, Wang P. A novel composite nonlinear controller for stabilization of constant power load in DC microgrid. *IEEE Transactions on Smart Grid* 2019; 10(1): 752–761.
14. Sulligoi G, Bosich D, Giadrossi G, Zhu L, Cupelli M, Monti A. Multiconverter medium voltage DC power systems on ships: Constant-power loads instability solution using linearization via state feedback control. *IEEE Transactions on Smart Grid* 2014; 5(5): 2543–2552.
15. Zhang X, Ruan X, Kim H, Chi KT. Adaptive active capacitor converter for improving stability of cascaded DC power supply system. *IEEE Transactions on Power Electronics* 2013; 28(4): 1807–1816.
16. Aronson DG, Ermentrout GB, Kopell N. Amplitude response of coupled oscillators. *Physica D: Nonlinear Phenomena* 1990; 41(3): 403–449.

17. Ermentrout GB. Oscillator death in populations of âĂIJall to allâĂİ coupled nonlinear oscillators. *Physica D: Nonlinear Phenomena* 1990; 41(2): 219–231.

18. Konishi K, Sugitani Y, Hara N. Dynamics of DC bus networks and their stabilization by decentralized delayed feedback. *Physical Review E* 2015; 91(1): 012911.

19. Hens C, Olusola OI, Pal P, Dana SK. Oscillation death in diffusively coupled oscillators by local repulsive link. *Physical Review E* 2013; 88(3): 034902.

20. Huddy SR, Skufca JD. Amplitude death solutions for stabilization of DC microgrids with instantaneous constant-power loads. *IEEE Transactions on Power Electronics* 2012; 28(1): 247–253.

21. Golnaraghi F, Kuo BC. *Automatic control systems*. McGraw-Hill Education . 2017.

22. El Aroudi A, Orabi M. Dynamics of PFC power converters subject to time-delayed feedback control. *International Journal of Circuit Theory and Applications* 2012; 40(1): 15–35.

23. Hassan MA, He Y. Constant power load stabilization in DC microgrid systems using passivity-based control with nonlinear disturbance observer. *IEEE Access* 2020; 8: 92393–92406.

24. El Aroudi A, Giaouris D, Mandal K, et al. Complex non-linear phenomena and stability analysis of interconnected power converters used in distributed power systems. *IET Power Electronics* 2016; 9(5): 855–863.

25. Zadeh MK, Gavagsaz-Ghoachani R, Martin JP, Pierfederici S, Nahid-Mobarakeh B, Molinas M. Discrete-time tool for stability analysis of DC power electronics-based cascaded systems. *IEEE Transactions on Power Electronics* 2017; 32(1): 652–667.

26. Maity S, Suraj Y. Analysis and modeling of an FFHC-controlled DC-DC buck converter suitable for wide range of operating conditions. *IEEE Transactions on Power Electronics* 2012; 27(12): 4914–4924.

27. Maity S, Tripathy D, Bhattacharya TK, Banerjee S. Bifurcation analysis of PWM-1 voltage-mode-controlled buck converter using the exact discrete model. *IEEE Transactions on Circuits and Systems I: Regular Papers* 2007; 54(5): 1120–1130.

28. Sun J, Mitchell DM, Greuel MF, Krein PT, Bass RM. Averaged modeling of PWM converters operating in discontinuous conduction mode. *IEEE Transactions on Power Electronics* 2001; 16(4): 482–492.

29. Ahamed AI, Lakshmanan M. Discontinuity induced Hopf and Neimark-Sacker bifurcations in a memristive Murali-Lakshmanan–Chua circuit. *Int. Jour. of Bifur. and Chaos* 2017; 27(06): 1730021.

30. Leine R, Van Campen D. Bifurcation phenomena in non-smooth dynamical systems. *European Journal of Mechanics-A/Solids* 2006; 25(4): 595–616.

31. M. di Bernardo , C. J. Budd , A. R. Champneys , P. Kowalczyk . *Piecewise-smooth Dynamical Systems: Theory and Applications*. Applied Mathematical Sciences: Springer . 2008.

32. Alexander J. C , Seidman T. I . Sliding modes in intersecting switching surfaces I: Blending. *Houston Journal of Mathematics* 1998; 24(3): 545–569.

33. Alexander J. C , Seidman T. I . Sliding modes in intersecting switching surfaces II: Hysteresis. *Houston Journal of Mathematics* 1999; 25(1): 185–211.

34. Zou W, Senthilkumar D, Duan J, Kurths J. Emergence of amplitude and oscillation death in identical coupled oscillators. *Physical Review E* 2014; 90(3): 032906.